Composites: Part A 150 (2021) 106591

Contents lists available at ScienceDirect

Composites Part A

journal homepage: www.elsevier.com/locate/compositesa

Flexible anisotropic magneto-sensitive elastomer films with out-of-plane particle chain for bionic actuator

Jingyi Zhang [a], Yu Wang [a,*], Haoming Pang [a], Shuaishuai Sun [b], Zhenbang Xu [c], Longjiang Shen [d], Xufeng Cao [a], Chuanlin Sun [a], Bochao Wang [a], Xinglong Gong [a,*]

[a] CAS Key Laboratory of Mechanical Behavior and Design of Materials, Department of Modern Mechanics, CAS Center for Excellence in Complex System Mechanics, University of Science and Technology of China (USTC), Hefei 230027, PR China
[b] Department of Precision Machinery and Instrumentation, University of Science and Technology of China (USTC), Hefei 230027, PR China
[c] CAS Key Laboratory of On-orbit Manufacturing and Integration for Space Optics System, Changchun Institute of Optics, Fine Mechanics and Physics, Chinese Academy of Sciences, Changchun 130033, PR China
[d] Hunan Bogie Engineering Research Center, Zhuzhou 412000, PR China

ARTICLE INFO

Keywords:
Smart materials
Thin films
Anisotropy
Mechanical properties
Magnetic properties

ABSTRACT

Owing to the flexible and controllable characteristics, the magnetic composite film becomes an ideal option for future portable, efficient and multifunctional magnetic soft actuators. Here, an anisotropic magneto-sensitive elastomer film (MSEF) composite based on polydimethylsiloxane (PDMS) and high concentration of carbonyl iron particles (CIPs) was developed. The off-plane design of CIP structures endows MSEF excellent field-dependent deformability and actuation ability. The off-plane bending angle of the MSEF-30° in 87mT uniform magnetic field could reach 70.78°. Moreover, the MSEF-20° could lift a heavy object 66.4 times its own weight. The influences of particle chain orientation, CIP contents, thickness and applied magnetic field on the magneto-induced deformation behavior were fully discussed, and finite element calculations were performed to clarify the experimental results. An improved balance equation was proposed and qualitatively explained the experimental results under different magnetic fields. Based on the MSEF composite, biomimetic soft actuators with bidirectional deformation and self-sensing functions were produced respectively. The two easy preparation and programmable soft actuators could achieve the expected actuation effect, indicating that the anisotropic MSEFs have great potential as soft actuators in the fields of biomedicine, microfluidics, intelligent robots and bionics applications.

1. Introduction

Compared with traditional rigid actuators, the soft actuators, with the superior flexibility, adaptability and deformability, have great potential in the field of biomedicine [1], health monitoring [2,3], MEMS device [4] and soft robot [5,6]. Various soft actuators have been designed and fabricated based on different stimuli-responsive mechanism [7–11]. Among them, the magnetically controlled soft actuators based on magneto-sensitive elastomer materials have attracted growing attentions [12–15]. Magneto-sensitive elastomer materials are usually fabricated by incorporating micron or nanometer magnetic particles into continuous polymer matrix [16,17]. By varying external magnetic field, the magnetic polymer composite materials behave elongation, contraction, bending and twisting [7,18–21]. The deformation can be achieved with fast response time, small size of device, high power efficiency and low drive voltages, etc [22]. As a result, magneto-sensitive soft actuators have been found in mechatronic and micro-robotic systems [13,23].

As one kind of magneto-sensitive elastomer, anisotropic magneto-sensitive elastomer film (MSEF) has extraordinary deformability under external magnetic field due to its high saturated magnetization, low stiffness and high flexibility [12,24–26]. Therefore, the anisotropic MSEF composite is very suitable for developing the intelligent actuators. Zhang et al. [27] fabricated magnetically actuated three-dimensional mobile microgripper based on the programmable magnetic-sensitive elastomer film. By directly controlling the magnetic force and torque applied to the microgripper, the micro objects could be grasped and transported. Mishra et al. [28] utilized nanoparticle chains oriented in

* Corresponding authors.
E-mail addresses: wyu@ustc.edu.cn (Y. Wang), gongxl@ustc.edu.cn (X. Gong).

https://doi.org/10.1016/j.compositesa.2021.106591
Received 4 May 2021; Received in revised form 20 July 2021; Accepted 5 August 2021
Available online 9 August 2021

plane and prepared the magnetic elastomer films with anisotropic mechanical response, which enabled the direction-controlled actuation under magnetic field. Schmauch et al. [29] concluded that the chained magnetic microparticles (MMPs) could provide more complex deformation behaviors for soft actuators. The magnetically actuated lifters, valves, and peristaltic pumps were fabricated to demonstrate their capabilities in different work status based on the elastomer films with chained MMPs.

In previous studies, the flexible MSEFs with the magnetic particle chains arranging within the plane were connected to obtain micro actuators. During the pre-structured process of the magnetic sensitive elastomer film, the attractive dipolar interactions pull the magnetic particles together to form chains. One-dimensional arrangement of magnetic particle chains will bring the composite the magnetic anisotropy. The magnetic particle chains are magnetized much more when the chain orientation is parallel to the external magnetic field direction. Consequently, the alignment of the chains along the external magnetic field direction is energetically favorable and the magnetically induced mechanical response is orientation-dependent [28]. The bending, curling and other complex motions under uniform magnetic fields are achieved by magnetic anisotropy [30]. However, there are some unavoidable problems in MSEFs composed of in-plane particle chains. The changes of particle chain orientation will cause composite membrane the combined deformation of bending and torsion [28]. Some special measurement techniques are required to quantitatively investigate the magneto-deformation. In addition, excessive magnetic inclusions in-plane can eliminate the magnetic anisotropy caused by the chain arrangement of particles. Only composite films with magnetic particle mass fraction less than 10.2% have been studied [29].

Therefore, the anisotropic magnetic sensitive elastomer films with particle chain orientation along the thickness direction were investigated in this paper. The distribution of micron magnetic particles inside the MSEF was observed by the X-ray microtomography. Under different magnetic fields, the influence of contents, chain orientation and magnetic field strength on the deformation of the MSEF was explored experimentally. And then, a modified model for magnetically induced deformation was proposed based on magneto-elastic theory. Moreover, the actuation force of the MSEF composite as soft actuator was also evaluated by lifting different loads. Finally, a bidirectional actuator and a self-sensing actuator composed of MSEFs were fabricated, indicating the great potential of MSEFs in the soft actuators field.

2. Experiment

2.1. Materials

The polydimethylsiloxane (PDMS) precursor and curing agent (Sylgard 184) were purchased from Dow Corning. The carbonyl iron particles (CIPs) with average size 7 μm were brought from BASF in Germany. All the reagents were analytically pure and were adopted without additional purification.

2.2. Preparation

First, the PDMS precursor and the curing agent at a mass ratio of 10:1 were mixed. Second, the CIPs were added into the mixture (Fig. 1). The three components were stirred with a glass rod for 10 min to mix thoroughly. The mixture was treated by vacuum oven for 10 min to remove bubbles. Then, the mixture was transferred to the surface of silicon wafer (50 mm × 50 mm). With spin coater 1000 rpm rotated speed for about one and half minutes, the mixture covered the silicon wafer evenly. After that, a pre-structured magnetic field was applied on the silicon wafer with the uniform distributed mixture for 10 min. At the end, the silicon wafer was heated at 100℃ for 10 min on the heating plate. The magnetic-sensitive elastomer composite film was then carefully peeled off from the silicon wafer.

With the same procedure, the MSEFs with 20%, 30%, 40% and 50% CIPs mass fraction were fabricated. Meanwhile, during the pre-structured process, the silicon wafer was set to along the different direction with the external magnetic field to obtain the film with different orientations of magnetic particle chains (Fig. S1). The strength of pre-structured magnetic field is 10mT, 20mT, 30mT and 40mT respectively. The samples with tilt angle of 0°, 10°, 20° and 30° were prepared, which were respectively named as MSEF-0°, MSEF-10°, MSEF-20° and MSEF-30° in the following contents.

2.3. Characterizations

To observe the microstructure of MSEF, X-ray microtomography (Xradia 520 Versa, Carl Zeiss X-ray Microscopy, Inc., USA) with 1024 ×

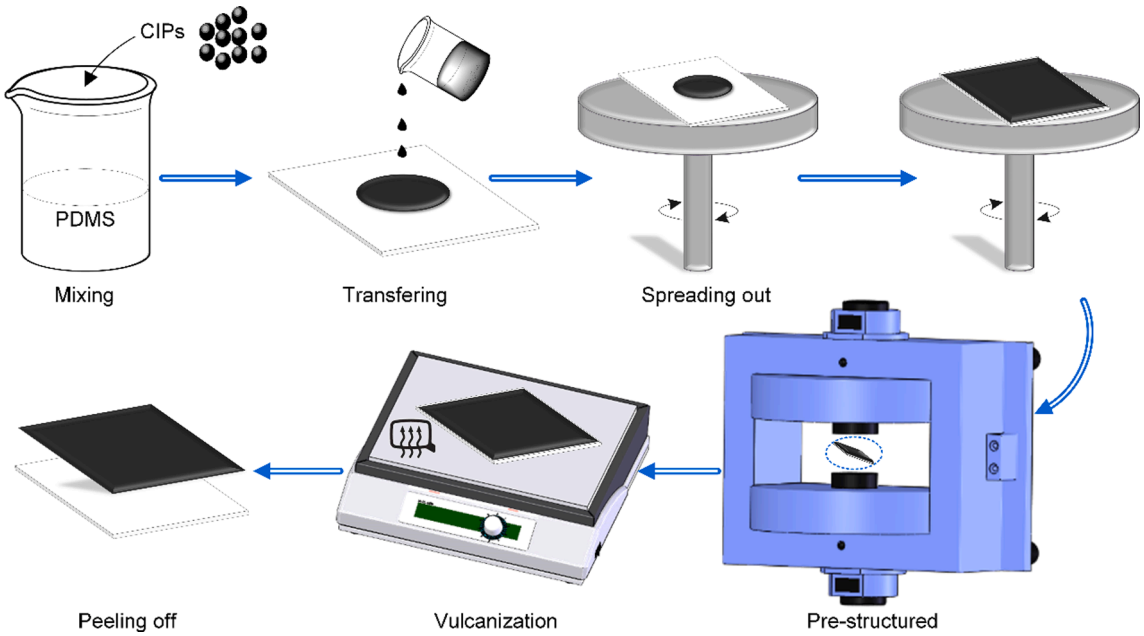

Fig. 1. Manufacturing process of MSEF. (For interpretation of the references to colour in this figure legend, the reader is referred to the web version of this article.)

1024 pixels, of which the pixel size was about 0.7 μm, was used to provide three-dimensional image of the particle distribution (Fig. 2a). The optical microscope (OM, VHX-200) was also employed to view the relative position of the particles and the matrix on the cross section. The film thickness was measured by the OM image. The thickness of each sample was measured 5 times at different positions. The arithmetic mean of results was defined as the final thickness value.

A self-made platform was built to measure the deformation of the magneto-sensitive elastomer composite film (Fig. 3a). The electromagnets (XDA-120/70, Yueqing Xingda Electric Co., Ltd., China) were exploited to generate the external magnetic field. The magnetic field strength was controlled by the current of power supply (ITECH IT6724). The sample was glued on the L-shaped glass shelf. A 3D printed plastic support was utilized to fix the electromagnets and the glass shelf. The deformation image was recorded by camera. The image was recognized to obtain the spatial configuration of film under different external magnetic fields.

Tensile test of MSEF was conducted on an electroforce dynamic system (TA ElectroForce 3220, TA Instruments). The magnetic hysteresis loops of MSEFs were characterized by a magnetic property measuring system vibrating sample magnetometer (SQUID, Quantum Design Co., America). The multiphysics modeling and simulation software COMSOL was used to calculate the distribution of the test magnetic field and the deformation of the MSEF.

3. Results and discussion

3.1. Microstructure of MSEF composites

The microstructures of different samples were observed by the X-ray microtomography. Two typical results are shown in Fig. 2b and 2c. It can be clearly seen that most of the CIPs in the MSEF-0° sample with wt50% CIPs are arranged into chain and distributed along the thickness direction in the matrix. While, as for the sample of MSEF-20° with wt20% CIPs (Fig. 2c), the particle chains are formed in the oblique direction with the normal direction of the film surface, of which the average angle is about 20°. Fig. 2d–f show the cross-section OM photos of MSEFs-20° with wt20%, wt30% and wt40% CIPs. The white dots represent magnetic particles. It can be seen that the larger the mass fraction of iron powder, the more spots on the cross section of the film. From the observation results, the arrangement orientations of particle chain in the samples meet the expectation by pre-design in the pre-structured process.

3.2. Deformation of MSEF composites under the uniform magnetic field

Fig. 3a shows the test system for magnetically induced deformation under the uniform magnetic field. The magnetic flux density at the center of the two electromagnets was measured with a digital tesla meter (HT20, Shanghai Hengtong Magnetic Technology Co., Ltd., China). The magnetic field strength has a linear relationship with the current (Fig. S2). In order to inspect the uniformity of the experimental magnetic field, electromagnets with the same proportion were simulated in COMSOL software. The parameters used are shown in Table S1. The calculation results with the control current at 0.9A are exhibited in Fig. 3b. It is obvious that the magnetic field around the sample position is uniform and the magnetic field direction is along the z-axis direction.

Next, the MSEF-20° sample was glued on the L-shape shelf in the test platform. The magnetically induced off-plane deformation of the sample was measured under different external magnetic fields. As shown in Fig. 3a, the red line is the deformation spatial configuration of the sample and the dotted black line represents the connection line between the free end and fixed end. The angle of the connection line with the y-axis is defined as the deformation angle φ, which can be used to describe the magnetically induced deformation capability of film. As seen from the Fig. S3, the deformation angle φ of MSEF-0° sample is nearly zero under the same magnetic field, which means that the oblique magnetic particle chains greatly affect the magnetically induced deformation of the magneto-sensitive elastomer film.

The size effects are discussed in Fig. 3c. It shows that, with different ratios of length to width, the deformation angles almost have the same value under different external magnetic fields. The deformation angle of the MSEF increases with the magnetic flux density increasing. The deformation angles of films with other sizes were also tested. There is little difference in the maximum deformation angle (Fig. S4a). In addition, the hysteresis behavior of the magnetic induced deformation is shown in Fig. 3d and Fig. S4b–d. It can be found that there is a hysteresis phenomenon during the loading cycle of external magnetic field. The deformation behaviors of three samples with same size and different particle chain orientations under the magnetic flux density cycling are

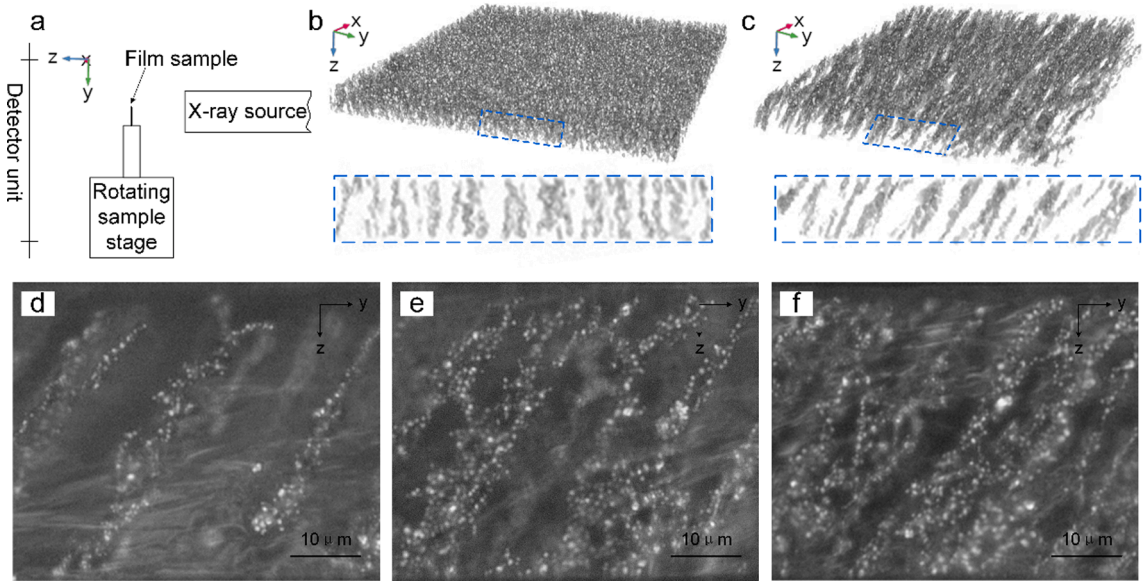

Fig. 2. (a) The schematic diagram of X-ray microtomography. Ct scan results of (b) Orthotropic MSEF-0° sample with wt50% CIPs and (c) MSEF-20° with wt20% CIPs. The OM images of MSEFs-20° with (d) wt20%, (e) wt30% and (f) wt40% CIPs. (For interpretation of the references to colour in this figure legend, the reader is referred to the web version of this article.)

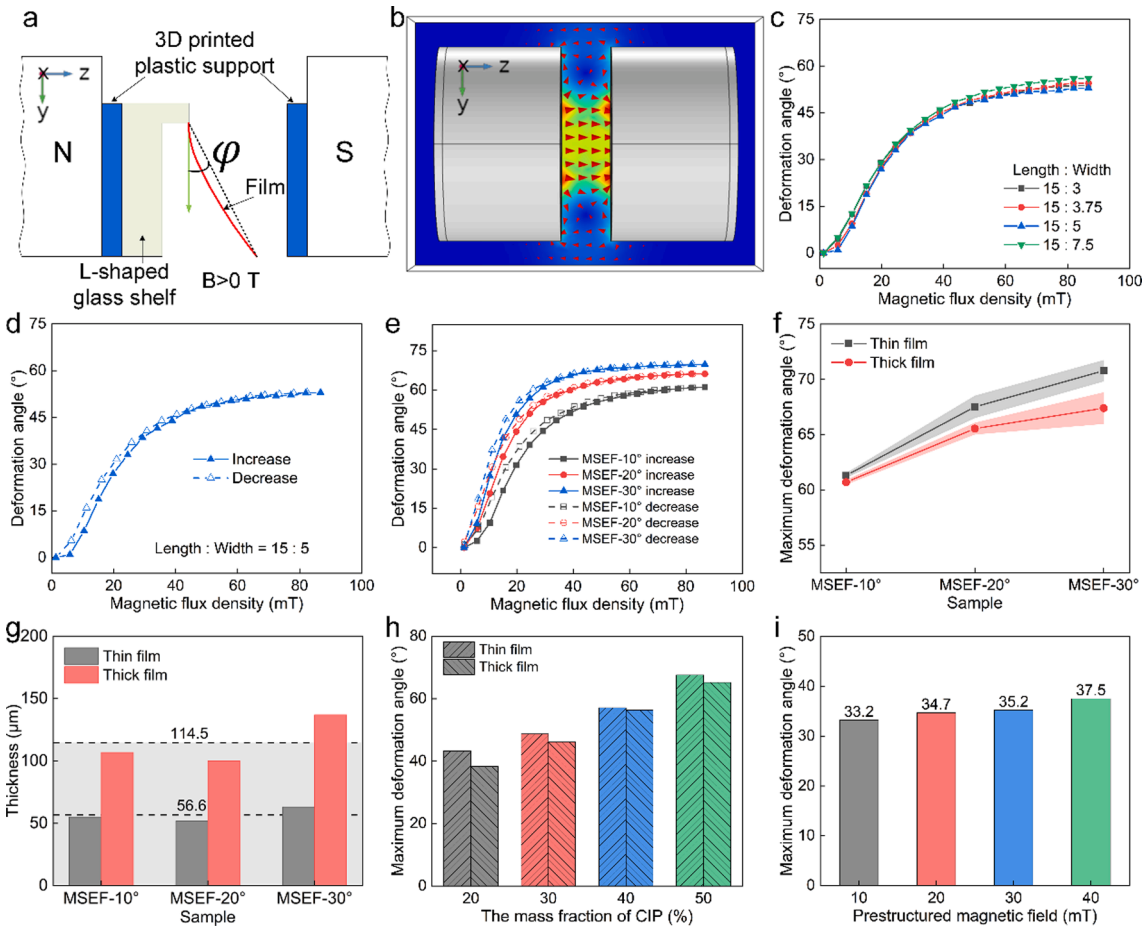

Fig. 3. (a) The schematic of uniform magnetic field generator and the deformation of MSEF-20° (15 mm × 5 mm × 0.05 mm, CIPs wt20%). (b) The simulation results of magnetic field. The arrows represent the magnitude and direction of the magnetic field. Influencing factors of magneto-induced deformation under uniform magnetic field. (c) The aspect ratio of film. (d) Application and removal of magnetic field. (e) The orientation of particle chain. (f) (g) The thickness of composite film. (h) The mass fraction of CIPs. (i) The strength of the pre-structured magnetic field. (For interpretation of the references to colour in this figure legend, the reader is referred to the web version of this article.)

summarized in Fig. 3e. It displays that the MSEF-30° has the largest deformation angle while the MSEF-10° has the smallest one. Meanwhile, as shown in Fig. 3f, the thinner films always have higher maximum deformation angle due to the less bending stiffness. The thickness of each sample in Fig. 3f is shown in Fig. 3g. As observed from the cross-section images of optical microscope (Fig. 2d–f), the number of internal particle chains increases with the CIPs mass fraction. Consequently, the torque caused by the dipolar interaction in the magnetic particle chain will be raised, which leads to the increment of magneto-induced deformation angle (Fig. 3h). As previous reported, a stronger pre-structured magnetic field would also increase the number of magnetic particle chain [17]. Therefore, the sample of MSEFs-20° fabricated under a higher pre-structured magnetic field will have a larger deformation angle (Fig. 3i).

3.3. Deformation of MSEF composites under gradient magnetic field

Furthermore, the deformation behaviors of MSEF were investigated on the non-uniform magnetic field platform (Fig. 4a). The non-uniform magnetic field was realized by a single electromagnet. Fig. S5a manifests that there is a linear relationship between the magnetic flux density and the supply current. From the simulation results shown in Fig. S5b, it can be confirmed that there is a gradient magnetic field. It can be seen from Fig. S6a and b that the magnetic field strength is only related to the variation of z and irrelevant to the variable y. Therefore, the changes of magnetic field strength are mainly controlled by varying the distance between the sample and the electromagnet along the z direction.

The deformation angle in the non-uniform magnetic field was measured and shown in Fig. 4b and c. The samples are MSEF-0° and MSEF-20° with wt20% CIPs. The current of external magnetic field keeps constant at 1.9A. Fig. 4b shows that, with the increase of distance z, the deformation angle of MSEF-0° increases firstly and then decreases. Comparing the results exhibited in Fig. 4b and Fig. S3, the MSEF-0° sample hardly deforms under the uniform magnetic field, but has obvious field-dependent deformation under the non-uniform magnetic field. It can be seen from Fig. 4c that the deformation angle of MSEF-20° shows a continuous decline with the distance z increasing. Moreover, the deformation direction of the MSEF-20° is opposite to that of MSEF-0°. Interestingly, once the glass frame with film was rotated by 180° (Fig. 4d), MSEF-20° deforms in another direction (Fig. 4f) but the deformation of MSEF-0° sample remains unchanged (Fig. 4e). In order to verify these experimental results, the deformation of MSEF-0° and MSEF-20° and MSEF-20° rotated by 180° (10 mm × 3 mm × 0.05 mm, CIPs wt20%) are calculated by software (Fig. 5b–d). The material parameters can be obtained from Fig. S6c and d. The geometric model is shown in Fig. 5a and relevant parameters can be referred to Table S2. Consistent with the experimental conditions, the MSEF is 15 mm away from the surface of the electromagnet, and the upper edge of the film is constrained. The calculated results, shown in Fig. 5e–g, are almost consistent with the experimental phenomenon.

Under uniform magnetic field, the MSEF is only subject to magnetic torque. For the MSEF-0° sample, the particle chain orientation is

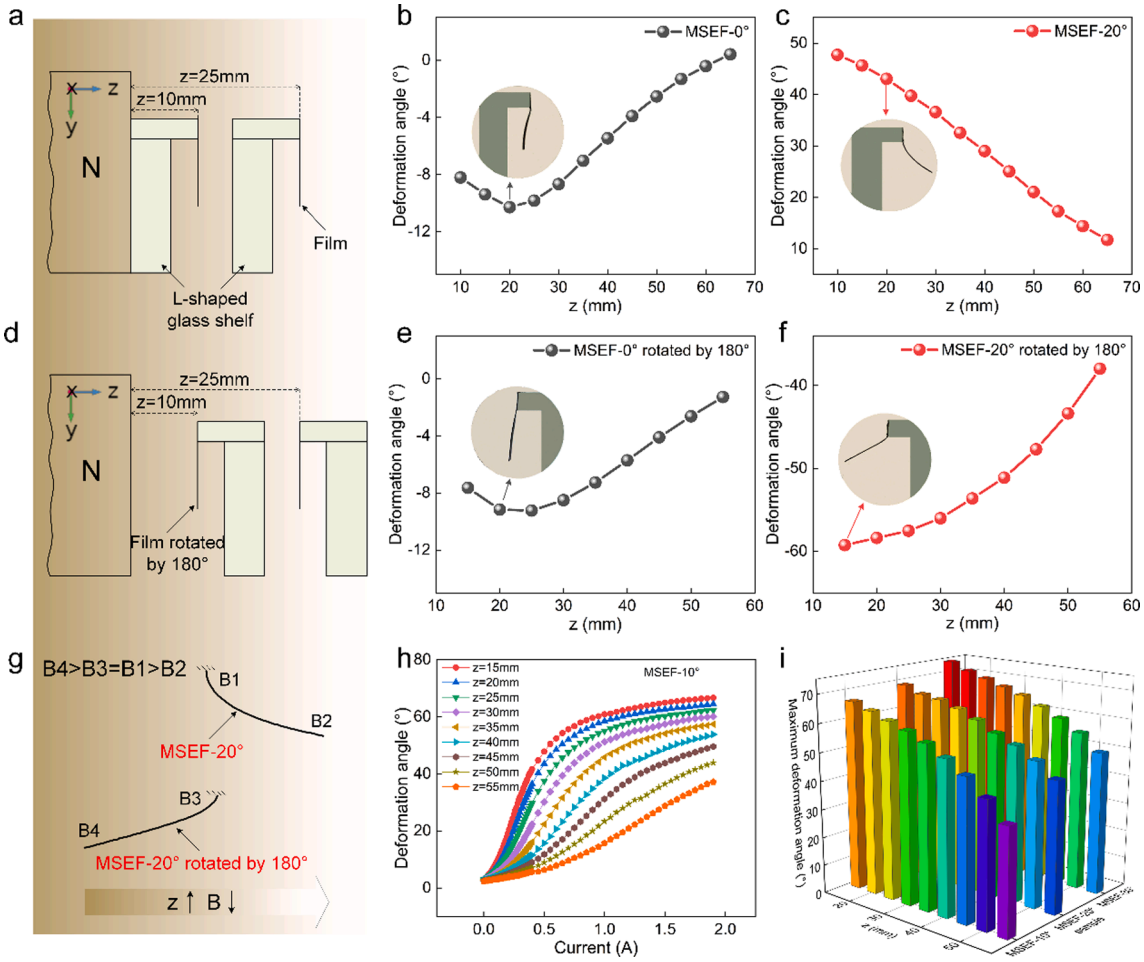

Fig. 4. (a) The MSEF and (d) the MSEF rotated by 180° are in the same inhomogeneous magnetic field environment, respectively. The deformation angles of (b) orthotropic MSEF-0° and (c) MSEF-20° (10 mm × 3 mm × 0.05 mm, CIPs wt20%) under 1.9A current at different positions z. (e) (f) The result after the L-shaped glass frame with composite film was rotated by 180° according to (b) (c). (g) The comparison about the deformation of MSEF-20° sample and MSEF-20° rotated by 180° sample. (h) The relationship between the current and deformation angles of MSEF-10° (10 mm × 3 mm × 0.05 mm, CIPs wt50%). (i) The influence of the distance z and the particle chain orientation on the deformation when the current is 1.9A. (For interpretation of the references to colour in this figure legend, the reader is referred to the web version of this article.)

consistent with the direction of the magnetic field, and the torque is 0. Therefore, the MSEF-0° sample hardly deforms under the uniform magnetic field. Under the non-uniform magnetic field, the composite film is simultaneously subjected to magnetic torque and magnetic field gradient force. For MSEF-0° sample, it is mainly affected by the magnetic field gradient force and deforms in the direction of force. If the magnetic field does not change, the deformation direction of the sample will not change. For MSEF-20° sample, the magnetic torque is dominant. The magnetic torques make particle chains deflect into the magnetic field direction (anticlockwise). When MSEF-20° sample is rotated by 180°, the direction of the magnetic torque on the particle chain will be changed (clockwise). Consequently, the deflection direction would be opposite.

When the distance is the same, the deformations of MSEF-20° sample and MSEF-20° rotated by 180° sample are not symmetrical under the same magnetic field (Fig. 4g). In the deformed configuration of MSEF-20°, the magnetic field is stronger at the fixed end and smaller at the free end. However, for the MSEF-20° rotated by 180° sample, the magnetic field on the fixed end is smaller than that on the free end. Fig. 4h, Fig. S7a and S7b show the relationship between the deformation angle and the current. At the same distance, the deformation angle increases with the current. When the current is constant, the deformation angle shows decrease with the distance increasing. The increase of current and the decrease of distance will increase the strength of the ambient magnetic field, so the deformation angle will increase. The results about MSEF-0° sample are shown in Fig. S7c. It can be found that the deformation angle of MSEF-0° sample is always smaller than that of MSEF-20° rotated by 180° sample. The combined effect of distance and internal structure on deformation angle is summarized in Fig. 4i. The deformation angle is largest when MSEF-30° is subjected to a strong magnetic field.

3.4. Mechanism of magnetically induced deformation

Deformation mechanism diagram of the MSEF with oblique magnetic particle chain under uniform magnetic field is shown in Fig. 6. Projecting to the y-z plane, the film can be regarded as cantilever beam with upper end fixed. Internal particle chains are simplified into red lines (Euler coordinate system) with same angle $\varphi_{initial}$(Fig. 6a). The number and spacing of the red lines depend on the particle content.

It is assumed that after the film deforms, the orientations of the particle chains in it remain parallel in Euler coordinate system (Fig. 6d). The magnetic torque τ_i on a particle chain can be obtained by deriving the magnetic dipole interaction [20]:

$$\tau_i \approx \frac{3\mu_0 m^2 n^2}{4\pi d^3}\sin 2\alpha \tag{1}$$

Here m is the magnetic moment. m = MV, M and V are the

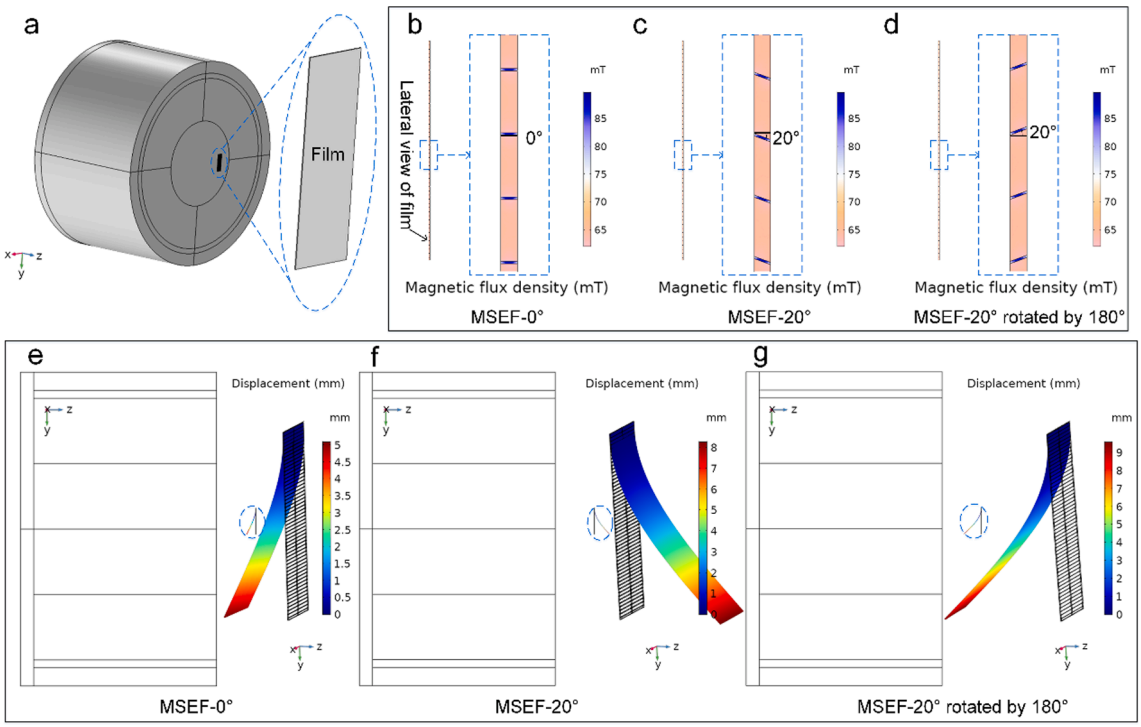

Fig. 5. (a) Schematic diagram of the relative position of electromagnet and film in COMSOL. (b–d) Local enlargement about the cross section of the film. The slender parts with higher magnetic flux densities in the photos represent the locations of the particle chains. The deformation results of (e) orthotropic sample and (f) MSEF-20° and (g) MSEF-20° rotated by 180° through calculation. (For interpretation of the references to colour in this figure legend, the reader is referred to the web version of this article.)

magnetization and volume of the particle, respectively. n represents the number of particles in a particle chain. μ_0 is the vacuum permeability and d is the inter-particle distance. α represents the angle between the direction of the particle chain and the external magnetic field (Fig. 6b and Fig. 6d).

$$M = \chi H \tag{2}$$

χ represents the magnetic susceptibility of a particle, and H is the external magnetic field intensity.

The total magnetic torque on the film with N particle chains is (counterclockwise):

$$\tau_{total} = N\tau_i = N\frac{3\mu_0 m^2 n^2}{4\pi d^3}\sin 2\alpha = N\frac{4\mu_0 n^2 \chi^2 R^6 \pi}{3d^3}H^2 \sin 2\alpha \tag{3}$$

R is particle radius.

One the other hand, according to the deflection formula of cantilever beam only subjected to the bending moment, the relationship between the deformation angleφ and the elastic restoring moment is (Fig. 6c):

$$\tau_{mech} = -\frac{2EI_x}{l}\varphi \tag{4}$$

E,I_x and$l$ are elastic modulus, inertia moment and length of the beam, respectively.

Initially, the sample with particle chain orientation angle $\varphi_{initial}$ bends due to the magnetic moment (Fig. 6b). As the bending deformation increases, the angle α and the magnetic moment decreases (Fig. 6d). On the contrary, the elastic restoring moment would increase due to the increase of deformation angleφ (Fig. 6c). Until the magnetic moment and the restoring moment reach equilibrium, the film reaches the deformed configuration. Therefore, in the deformed configuration (Fig. 6d), the equilibrium equation would be:

$$N\frac{4\mu_0 n^2 \chi^2 R^6 \pi}{3d^3}H^2 \sin 2\alpha = \frac{2EI_x}{l}\varphi \tag{5}$$

The geometric relationship is $\alpha = \varphi_{initial} - \varphi$. Then, the Eq. (5) becomes:

$$N\frac{4\mu_0 n^2 \chi^2 R^6 \pi}{3d^3}H^2 \sin 2(\varphi_{initial} - \varphi) = \frac{2EI_x}{l}\varphi \tag{6}$$

From the above equation, the relationship between magnetic field strength$H$ and deformation angle φ is not linear. Their relationship is affected by the initial particle chain orientation, the particle content, the bending stiffness of the film, inter-particle distance, the magnetic susceptibility and the radius of the particle.

According to the magnetic dipole interaction energy, the sample tends to bend into the deformed configuration to achieve particle chain aligning along the H direction ($\alpha = 0$) where magnetic dipole interaction energy is minimum, which is independence of the strength of H. When the particle chain is arranged in the magnetic field direction, the magnetic torque on the particle chain is 0 and the film hardly deforms even the magnetic flux density is large. Therefore, the deformation angle φ eventually reaches a plateau value as the external magnetic field increases. The case that after bending deformation the angle α is no longer the same was also considered (Fig. S8).

The analytical model of film deformation under non-uniform magnetic field is shown in Fig. 7b. According to equation (S3), the magnetic moment (counterclockwise) is:

$$\int_0^s \frac{\mathrm{N}}{l}\bullet\frac{4\mu_0 \mathrm{n}^2 \chi^2 \mathrm{R}^6 \pi}{3\mathrm{d}^3}(\mathrm{H_z(s)})^2 \sin 2[\varphi_{\mathrm{initial}} - \theta(\mathrm{s})]\mathrm{ds} \tag{7}$$

For calculating the magnetic force, the film per unit length is regarded as uniform magnetic medium with magnetic susceptibility χ_s (Fig. 7c).χ_s depends on the magnetic susceptibility χ and content of the CIP. Magnetic field gradient force $\boldsymbol{F}$ can be given as:

$$\boldsymbol{F} = \mu_0 \chi_s \mathrm{V}(\boldsymbol{H}\cdot\nabla)\boldsymbol{H} \tag{8}$$

V are the volume of magnetic medium. Therefore, the magnetic force per unit length of the film is:

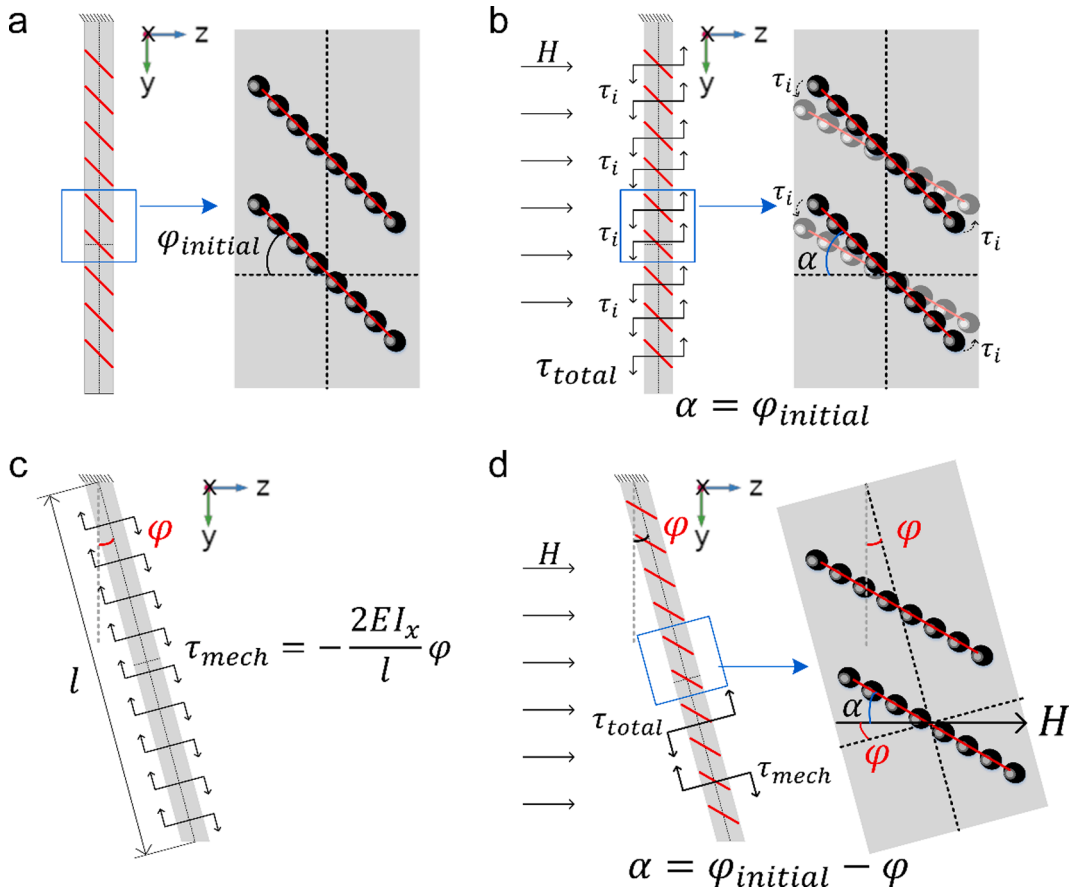

Fig. 6. (a) The projection of the film onto y-z plane. The particle chain is represented by red line, and its initial orientation angle is $\varphi_{initial}$. (b) Under the external magnetic field H, the particle chains on the film are subjected to magnetic torque τ_{total}. (c) The cantilever beam only subjected to the bending moment. (d) In the deformed configuration, the magnetic torque and the elastic recovery torque are balanced. (For interpretation of the references to colour in this figure legend, the reader is referred to the web version of this article.)

$$q_z(s) = \mu_0 \chi_s bh\left(\frac{H_x(s)\partial}{\partial x} + \frac{H_y(s)\partial}{\partial y} + \frac{H_z(s)\partial}{\partial z}\right)H_z(s) \tag{9}$$

Where b and h represent the width and thickness of the film.

The moment of the magnetic force (clockwise) on the length of ds_0 at point s_0 to point s can be written as (Fig. 7a):

$$q_z(s_0)ds_0 \bullet \int_{s_0}^{s} -\cos\theta(s_1)ds_1 \tag{10}$$

From expression (7) and (10), the equilibrium equation under gradient magnetic field is:

$$\int_0^s \frac{N}{l} \bullet \frac{4\mu_0 n^2 \chi^2 R^6 \pi}{3d^3}(H_z(s))^2 \sin 2[\varphi_{initial} - \theta(s)]ds + \int_0^s q_z(s_0)ds_0 \int_{s_0}^{s} \cos\theta(s_1)ds_1 = EI_x \frac{d\theta(s)}{ds} \tag{11}$$

Eq. (11) is the model about the bending deformation of magnetic film under non-uniform magnetic field. The gradient descent method can be used to iteratively solve$\theta(0)$, $\theta(s)$ and $q_z(s)$. If the initial angle of particle chain orientation is opposite, the magnetic moment and magnetic force are both clockwise (Fig. 7c and f). For MSEF-0°, the first term of the Eq. (11) can be ignored due to the magnetic torque of film is zero (Fig. 7e).

3.5. Actuation force of MSEF composites

Here, the own weight of MSEF sample as a reference was employed to check the lift ability of the film. Same number of PDMS elastomers (10 mm × 3 mm × 0.5 mm) are bonded on both sides of the MSEF to evaluate the actuation force under the uniform magnetic field (Fig. 8e). Fig. 8a–c show the relationship between the magnetic flux density and the deformation angle of the MSEFs with weights. The MSEF-30° can lift a heavy object 58.2 times its own weight. When the MSEF actuates the load, the magnetic torque is balanced with the moment derived from the system's gravity. Then the magnetic moment per unit mass of the MSEF can be calculated and the results are shown in Fig. 8d. Moreover, from Eq. (3), the magnetic torque is proportional to the square of the external magnetic field:

$$\tau_{total} = \beta B^2 \tag{12}$$

The coefficient is β. Where $\beta = N\frac{4n^2\chi^2R^6\pi}{3\mu_0 d^3}sin2\alpha$.

According to formula (12), the τ_{total} of MSEF with larger α should be larger when $0^\circ \le \alpha \le 45^\circ$, which is in good agreement with the experimental results (Fig. 8d). Five MSEFs-20° (3 mm × 3 mm × 0.106 mm) with wt20% CIPs were combined with the ecoflex10, then a bionic muscle that appeared the extension and contraction under the applied magnetic field was developed (Fig. 8f). The MSEF is smaller and requires a weaker magnetic field than the magnetically sensitive film actuators that we have known before, which is conducive to miniaturization and low energy consumption of the device.

3.6. Bidirectional actuator based on MSEF composites

Fig. 9a shows the fabrication of a bidirectional actuator using the MSEFs and PDMS films. By adjusting the internal structure of the MSEFs or the pre-strain of the PDMS substrate, three kinds of actuators are

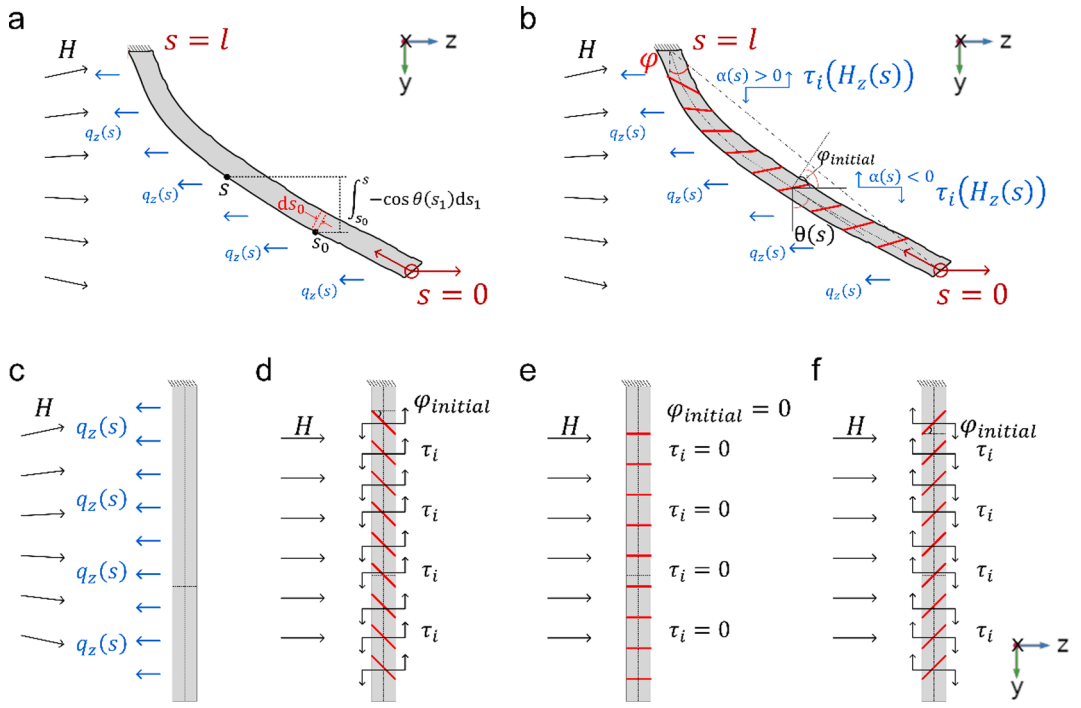

Fig. 7. (a) (b) The deformed configuration of the magnetic film under non-uniform magnetic field. (c) Magnetic force on the isotropic magnetic film under gradient magnetic field. (d–f) The relationship of magnetic moment and the initial orientation angle under uniform magnetic field. (For interpretation of the references to colour in this figure legend, the reader is referred to the web version of this article.)

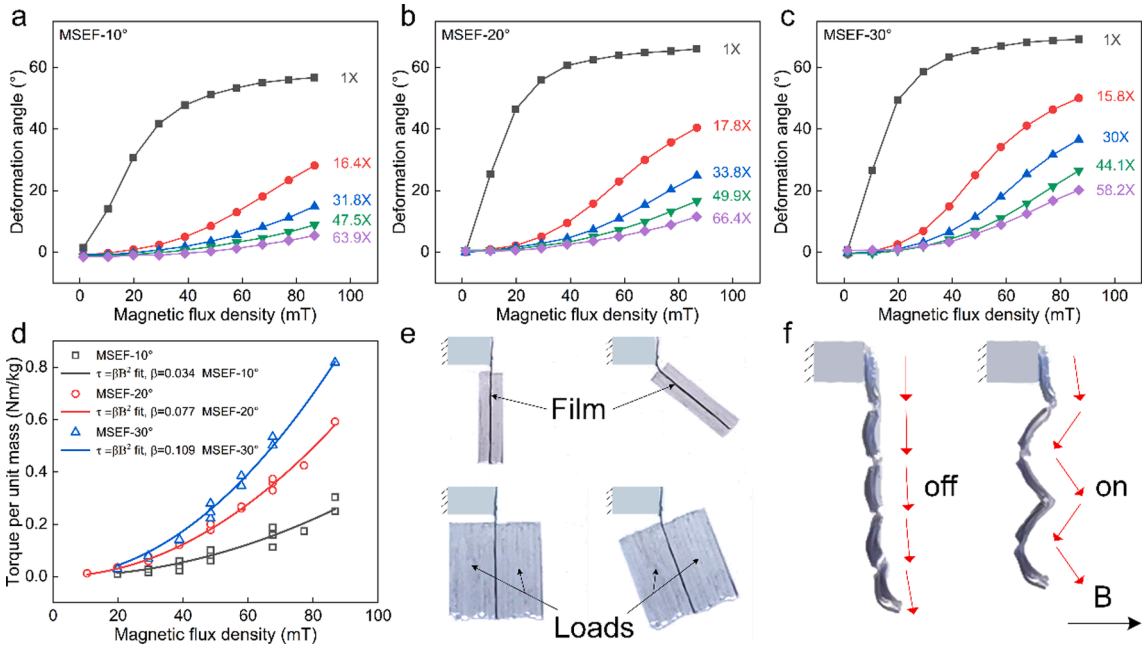

Fig. 8. The relationship between deformation and magnetic flux density when (a) the MSEF-10°, (b) the MSEF-20°, (c) the MSEF-30° is loaded with different weights. (d) The impact of magnetic field on the torque per unit mass of MSEFs. (e) The changes about the deformation of the MSEFs with different loads when responding to magnetic field. (f) Bionic muscle assembled of MSEFs. (For interpretation of the references to colour in this figure legend, the reader is referred to the web version of this article.)

prepared. The experimental results show that the bidirectional actuators are curved surface instead of plane in the initial state. After applying the magnetic field, the MSEFs suffer from different magnetic force and moment. Therefore, the bidirectional actuators exhibit various deformations.

The bidirectional actuator I with small curvature structure is placed on the electromagnet. After energizing the electromagnet, the bidirectional actuator I suffers outward magnetic torque and its deformation changes from concave to convex (Fig. 9a). Fig. 9a also exhibits that the MSEFs in the bidirectional actuator II with large curvature are subjected inward torque, which intensifies the bending deformation. Moreover, the outward deformation of the large-curvature actuator III is realized

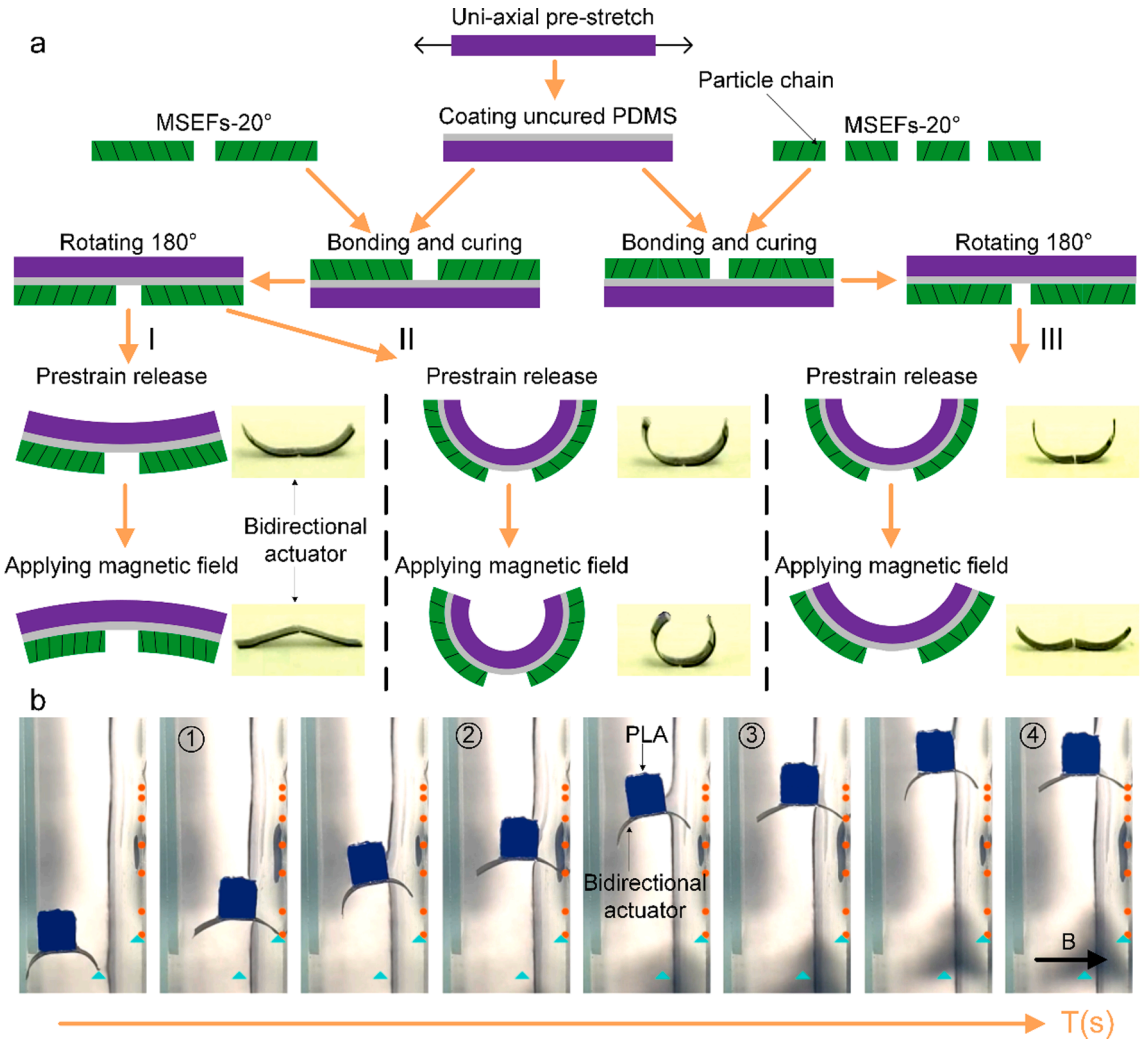

Fig. 9. (a) Preparation and deformation mechanism of bidirectional actuators based on MSEF. The insets show the experimental results of bidirectional actuator I with low curvature structure, bidirectional actuator II with high curvature structure and bidirectional actuator III with regional orientation of particle chains. (b) Sequence pictures that under intermittent magnetic field, the bidirectional actuator III acts as a fin and drives the entire structure to navigate on the water surface (vertical view). (For interpretation of the references to colour in this figure legend, the reader is referred to the web version of this article.)

through adjusting the particle chain orientation of the MSEFs (Fig. 9a). The simulations of the three bidirectional actuators are carried out in COMSOL, and the results are consistent with the experimental results (Fig. S9). Fig. 9b shows a bionic fish structure with actuator III as a fin and plastic PLA as a head, respectively. Under the action of intermittent magnetic field, the actuator III keeps switching between two steady states, causing disturbance to the surrounding flow field and promoting the bionic fish to swim on the water surface (Movie S1). Therefore, the bidirectional actuators are expected to be employed for simulating the swimming of jellyfish, scallop and fish, which is unimaginable for single deformation actuators. The bidirectional actuator enriches the application scenarios of the MSEF in the soft actuator, and the concept of bonding the MSEFs with different microstructures to the pre-stretched substrate is expected to inspire more multifunctional soft actuators.

3.7. *Self-sensing actuator based on MSEF composites*

Fig. 10a shows self-sensing actuator which is made of MSEFs-20° (14 mm × 10 mm × 0.05 mm, CIPs wt50%) and polyvinylidene fluoride (PVDF) (19 mm × 10 mm × 0.028 mm, Aimin Intelligent Co., China). The XRD result of PVDF exhibits the presence of β-phase, which proves the piezoelectricity (Fig. S10a). After bending, its upper and lower surfaces accumulate positive and negative charges respectively, resulting in potential difference. The upper and lower surfaces of PVDF film are respectively coated with silver paste to conduct the positive and negative charges. The aluminum wires drawn from the silver paste are electrodes to connect multimeter (DMM6000) for measuring the voltage that generates from the bending deformation of the PVDF film. Combining silver-PVDF-silver with MSEF actuator, the magnetic film acts as magnetically sensitive part and leads the whole structure to bend under uniform magnetic field. The silver-PVDF-silver bends synchronously to output electrical signal. According to the magnitude of the electrical signal, the deflection of the multilayered structure could be evaluated. The period of the external magnetic field square wave is 4 s, the magnetic field is dormant in first two seconds, and is turned on in next two seconds (Fig. 10b–c). Initially the voltage of the self-sensing actuator is 0. After magnetic field is applied, the self-sensing actuator deforms and the PVDF bends, generating low potential (V_min). Then the magnetic field does not change and the voltage returns to zero. At the end of the fourth second, the magnetic field is removed and the self-sensing actuator returns to the vertical state, generating positive potential (V_max). Finally, voltage returns to zero potential.

Fig. 10b and c display the voltage response of self-sensing actuator to the magnetic field strength. The insets show the voltage change of the actuator over time. When the magnetic flux density is lower than 49.6 mT, the changes of voltage could not be observed due to the minuscule

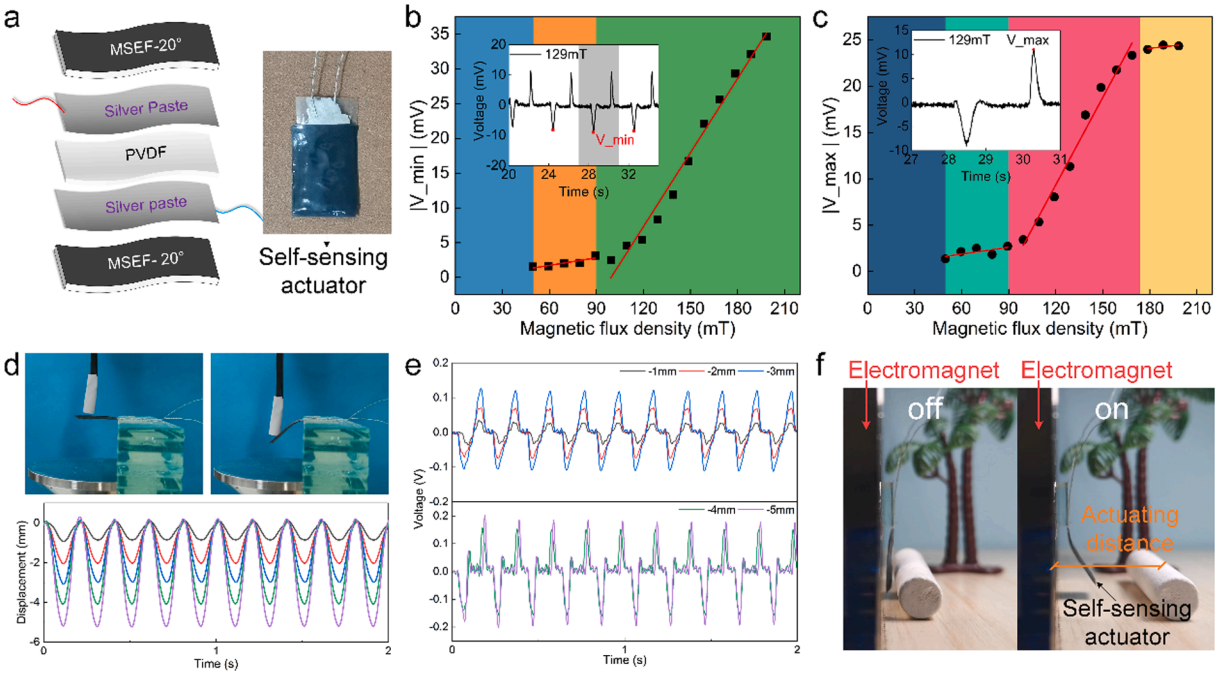

Fig. 10. Actuator with displacement-magnetic dual-mode sensing. (a) The structure of self-sensing actuator based on MSEF composite. (b)(c) Response to magnetic field. (d)(e) Response to displacement. (f) The actuation results of self-sensing actuator on the cylindrical chalk. (For interpretation of the references to colour in this figure legend, the reader is referred to the web version of this article.)

deformation of the actuator. In the second interval, the deformation of the self-sensing actuator is small, and the corresponding voltage signal is also small. When the external magnetic field is greater than 89.3 mT, V_min increases as the magnetic flux density increasing. However, V_max increases with the increase of the magnetic field and then tends to be stable. It might be caused by different deformation mechanisms. V_min occurs when the magnetic field is turned on. The magnetic field used for the test is much weaker than the magnetic field that saturates the particles. Therefore, the magnetic torque increases with the magnetic field, resulting the larger V_min. V_max appears when the magnetic field is removed. When the magnetic field is greater than 168.7mT, the increase rate of magneto-deformation decreases (Fig. S10b), so V_max tends to a fixed value. The self-sensing actuator is also evaluated under 952 magnetic field cycles and exhibits good durability (Fig. S10c).

The sensitivity of the self-sensing actuator to displacement was tested through the electroforce dynamic system (Fig. 10d). One end of the film is fixed, and the other end is controlled by displacement. Tests with a frequency of 5 Hz and amplitudes of 1 mm, 2 mm, 3 mm, 4 mm and 5 mm were carried out. Fig. 10e shows that the voltage of the film is positively correlated with the displacement excitation. The self-sensing actuator was placed near the electromagnet, and the magnetic field was applied to actuate non-magnetic objects with different shapes and sizes, such as cylindrical chalk (Fig. 10f) and glass balls (Fig. S11). The self-sensing actuator weighs 0.1253 g. The mass of chalk, big ball and small ball are 17.88 times, 11.71 times and 2.71 times that of actuator respectively. The piezoelectricity of PVDF endows the MSEF actuator with sensing function, which has practical significance for applications in vivo and in dangerous conditions.

4. Conclusion

In conclusion, anisotropic magneto-sensitive elastomer composite films with different off-plane angles and concentrations of magnetic particles were prepared. The internal microstructures of the composite films were observed by X-ray micro-tomography. A platform with an electromagnetic module, a structural support, and a camera was built to measure the magnetically induced deformation under different magnetic fields. The MSEF-30° sample exhibits 70.78° bending deformation angle under uniform magnetic field, which is much larger than the MSEF-0° sample. In inhomogeneous magnetic field, both experimental and simulation results show that after being rotated by 180°, MSEF-0° sample does not change the deformation direction, but MSEF-20° deforms in another direction. Under the 87mT uniform magnetic field, the MSEF-20° could lift a heavy object 66.4 times its own weight. The actuation torque has a quadratic relationship with the external magnetic field. The particle chain orientation, mass fraction, thickness, and the strength and gradient of the applied magnetic field will all affect the anisotropic deformation behavior and actuation ability of the MSEF, which endows the MSEF with programmable and controllable characteristics for soft actuators. A MSEF-based bidirectional actuator assembled from pre-strained substrate was produced and simulated fish swimming under intermittent magnetic excitation. A MSEF-based self-sensing actuator compounded with PVDF was also fabricated, which moved like a finger to clear various obstacles. Thus, the MSEFs as soft actuators that are critical to artificial muscles, soft robots and bionic applications can be developed.

CRediT authorship contribution statement

Jingyi Zhang: Conceptualization, Investigation, Writing – original draft. **Yu Wang:** Formal analysis, Funding acquisition, Writing – review & editing. **Haoming Pang:** Methodology, Visualization. **Shuaishuai Sun:** Investigation, Visualization. **Zhenbang Xu:** Investigation. **Longjiang Shen:** Investigation. **Xufeng Cao:** Software. **Chuanlin Sun:** Methodology. **Bochao Wang:** Investigation, Writing – review & editing. **Xinglong Gong:** Supervision, Project administration, Resources, Funding acquisition, Writing – review & editing.

Declaration of Competing Interest

The authors declare that they have no known competing financial interests or personal relationships that could have appeared to influence the work reported in this paper.

Acknowledgment

Financial supports from the National Natural Science Foundation of China (Grant No. 11972337, 11972343, and 52005474), the Anhui's Key R&D Program of China (202104a05020009), the National Key R&D Program of China (Grant No. 2018YFB1201703), the Strategic Priority Research Program of Chinese Academy of Sciences (Grant No. XDB22040502), and the Fundamental Research Funds for the Central Universities (WK2090000015, WK2480000009) are gratefully acknowledged. This work was partially carried out at the USTC Center for Micro and Nanoscale Research and Fabrication.

Appendix A. Supplementary material

Supplementary data to this article can be found online at https://doi.org/10.1016/j.compositesa.2021.106591.

References

[1] Dagdeviren C, Joe P, Tuzman OL, Park K-I, Lee KJ, Shi Y, et al. Recent progress in flexible and stretchable piezoelectric devices for mechanical energy harvesting, sensing and actuation. Extreme Mech Lett 2016;9:269–81.
[2] Lou Z, Li L, Wang L, Shen G. Recent progress of self-powered sensing systems for wearable electronics. Small 2017;13(45):1701791.
[3] Lin Y, Sodano HA. Concept and model of a piezoelectric structural fiber for multifunctional composites. Compos Sci Technol 2008;68(7-8):1911–8.
[4] Du G, Chen X. MEMS magnetometer based on magnetorheological elastomer. Measurement 2012;45(1):54–8.
[5] Hines L, Petersen K, Lum GZ, Sitti M. Soft actuators for small-scale robotics. Adv Mater 2017;29(13):1603483.
[6] Ding L, Xuan S, Feng J, Gong X. Magnetic/conductive composite fibre: A multifunctional strain sensor with magnetically driven property. Compos Part A-Appl S 2017;100:97–105.
[7] Qi S, Guo H, Fu J, Xie Y, Zhu M, Yu M. 3D printed shape-programmable magneto-active soft matter for biomimetic applications. Compos Sci Technol 2020;188:107973.
[8] Li W, Liu Y, Leng J. Light-actuated reversible shape memory effect of a polymer composite. Compos Part A-Appl S 2018;110:70–5.
[9] Yao Y, Zhou T, Wang J, Li Z, Lu H, Liu Y, et al. 'Two way' shape memory composites based on electroactive polymer and thermoplastic membrane. Compos Part A-Appl S 2016;90:502–9.
[10] Liu H, Tian H, Shao J, Wang Z, Li X, Wang C, et al. An electrically actuated soft artificial muscle based on a high-performance flexible electrothermal film and liquid-crystal elastomer. ACS Appl Mater Interfaces 2020;12(50):56338–49.
[11] Wang M, Li Q, Shi J, Cao X, Min L, Li X, et al. Bio-inspired high sensitivity of moisture-mechanical GO films with period-gradient structures. ACS Appl Mater Interfaces 2020;12(29):33104–12.
[12] Feng J, Xuan S, Ding L, Gong X. Magnetoactive elastomer/pvdf composite film based magnetically controllable actuator with real-time deformation feedback property. Compos Part A-Appl S 2017;103:25–34.
[13] Jeon J, Park JE, Park SJ, Won S, Zhao H, Kim S, et al. Shape-programmed fabrication and actuation of magnetically active micropost arrays. ACS Appl Mater Interfaces 2020;12(14):17113–20.
[14] Huang HW, Sakar MS, Petruska AJ, Pane S, Nelson BJ. Soft micromachines with programmable motility and morphology. Nat Commun 2016;7(1):12263.
[15] Zhang Z, Li X, Yu X, Chai H, Li Y, Wu H, et al. Magnetic actuation bionic robotic gripper with bistable morphing structure. Compos Struct 2019;229:111422.
[16] Yao J, Sun Y, Wang Y, Fu Q, Xiong Z, Liu Y. Magnet-induced aligning magnetorheological elastomer based on ultra-soft matrix. Compos Sci Technol 2018;162:170–9.
[17] Chen L, Gong XL, Li WH. Microstructures and viscoelastic properties of anisotropic magnetorheological elastomers. Smart Mater Struct 2007;16(6):2645–50.
[18] Gong X, Liao G, Xuan S. Full-field deformation of magnetorheological elastomer under uniform magnetic field. Appl Phys Lett 2012;100(21):211909.
[19] Guan X, Dong X, Ou J. Magnetostrictive effect of magnetorheological elastomer. J Magn Magn Mater 2008;320(3-4):158–63.
[20] Kim J, Chung SE, Choi SE, Lee H, Kim J, Kwon S. Programming magnetic anisotropy in polymeric microactuators. Nat Mater 2011;10(10):747–52.
[21] Zhang J, Pang H, Wang Yu, Gong X. The magneto-mechanical properties of off-axis anisotropic magnetorheological elastomers. Compos Sci Technol 2020;191:108079.
[22] Wu S, Hu W, Ze Q, Sitti M, Zhao R. Multifunctional magnetic soft composites: A review. Multifunctional Materials 2020;3(4):042003.
[23] Li J, Zhang M, Wang L, Li W, Sheng P, Wen W. Design and fabrication of microfluidic mixer from carbonyl iron–pdms composite membrane. Microfluid Nanofluid 2011;10(4):919–25.
[24] Zhang Q, Peng B, Li H, Sun J. Magnetically tunable transparency for magnetorheological elastomer films consisting of polydimethylsiloxane and Fe3O4 nanoparticles. Soft Mater 2018;16(3):220–7.
[25] Déry J-P, Brousseau D, Rochette M, Borra EF, Ritcey AM. Aluminum-coated elastomer thin films for the fabrication of a ferrofluidic deformable mirror. J Appl Polym Sci 2017;134(9).
[26] Sang M, Wang S, Liu M, Bai L, Jiang W, Xuan S, et al. Fabrication of a piezoelectric polyvinylidene fluoride/carbonyl iron (pvdf/CI) magnetic composite film towards the magnetic field and deformation bi-sensor. Compos Sci Technol 2018;165:31–8.
[27] Zhang J, Diller E. Tetherless mobile micrograsping using a magnetic elastic composite material. Smart Mater Struct 2016;25(11):11LT03.
[28] Mishra SR, Dickey MD, Velev OD, Tracy JB. Selective and directional actuation of elastomer films using chained magnetic nanoparticles. Nanoscale 2016;8(3):1309–13.
[29] Schmauch MM, Mishra SR, Evans BA, Velev OD, Tracy JB. Chained iron microparticles for directionally controlled actuation of soft robots. ACS Appl Mater Interfaces 2017;9(13):11895–901.
[30] Xu T, Zhang J, Salehizadeh M, Onaizah O, Diller E. Millimeter-scale flexible robots with programmable three-dimensional magnetization and motions. Sci Rob 2019;4(29):eaav4494.